Solid State Communications 283 (2018) 47–51

Contents lists available at ScienceDirect

Solid State Communications

journal homepage: www.elsevier.com/locate/ssc

Communication

Thermally activated flux creep in nanocrystalline δ-MoN thin films

N. Haberkorn[a,b,*], J.A. Hofer[b]

[a] Comisión Nacional de Energía Atómica and Consejo Nacional de Investigaciones Científicas y Técnicas, Centro Atómico Bariloche, Av. Bustillo 9500, 8400 San Carlos de Bariloche, Argentina

[b] Instituto Balseiro, Universidad Nacional de Cuyo and Comisión Nacional de Energía Atómica, Av. Bustillo 9500, 8400 San Carlos de Bariloche, Argentina

ARTICLE INFO

Communicated by J. Fontcuberta

Keywords:
A. Superconductors
B. Sputtering
D. Critical current densities
D. Flux creep relaxation

ABSTRACT

We study the vortex dynamics in a nanocrystalline 420 nm thick δ-MoN film on Si (100). The film was grown at room temperature by reactive sputtering and following it is crystallized by thermal annealing at 973 K for one hour. The microstructure shows grains with sizes between 30 nm and 65 nm. The film displays a T_c of 11.2 K. The magnetic field dependence of the critical current density J_c at intermediate and low fields (related to the upper critical field) displays a power-law regime. The self-field J_c at 4.5 K is ≈2 MA cm^{-2}. The pinning force F_p exhibits a maximum at $h \approx 0.3$, which is in agreement with vortex pinning produced by grain boundaries. An Anderson-Kim mechanism describes the temperature dependence of the flux creep rates. The U_0 values range from ≈2500 K for $\mu_0 H = 0.02$ T to ≈1300 K for $\mu_0 H = 0.5$ T.

1. Introduction

The most relevant technological applications of superconducting transition metal nitride thin films are radiation detectors and Josephson tunnel junctions [1,2]. Other less explored potential applications are related to current-carrying capability. Superconducting metal nitrides are chemically compatible with carbon-based structures, which allow improving vortex pinning [3,4] and facilitate the synthesis of thin films in light supports [5]. The δ-MoN phase displays superconducting critical temperatures T_c up 12 K [6]. In the superconducting dirty limit, the upper critical fields H_{c2} can be enhanced to values up 10 T (with weak crystalline anisotropy) [7,8]. δ-MoN thin films have been sintered by chemical [9,10] and physical methods [11]. The T_c in nanocrystalline samples is close to the bulk value, which simplifies the synthesis on polycrystalline substrates [11].

There are no reports related to vortex pinning in molybdenum nitride thin films. Most studies refer to NbN [12–14]. The vortex dynamics in a superconducting material is determined by intrinsic vortex fluctuations and by the geometry and density of the pinning centers [15]. The strength of vortex fluctuations is related to the Ginzburg number $Gi = \frac{1}{2}\left[\frac{\gamma T_c}{H_c^2(0)\xi^3(0)}\right]^2$ (γ anisotropy, and $H_c(0)$ and ξ(0) are the thermodynamic critical field and the coherence length at $T = 0$ K). The δ-MoN phase in the dirty limit is a material with $Gi \approx 1 \times 10^{-5} - 1 \times 10^{-6}$ ($T_c = 12$ K, λ ≈ 300–400 nm, ξ (0) = 6–7 nm and γ ≈ 1 [7,11]), which places it between conventional low temperature superconductors LTS ($Gi \approx 1 \times 10^{-8}$) and high temperature (HTS) and iron-based (IBS) superconductors ($Gi \approx 1 \times 10^{-5}$ – $Gi \approx 10^{-2}$). LTS present low vortex relaxation rates as consequence of pinning energies of thousands of Kelvins (described by Anderson-Kim [16]). The increment of the thermal fluctuations in HTS and IBS reduces considerably U (tens to hundreds of Kelvins), which rises considerably the flux creep rates (described by the collective pinning theory [15]). In this context, the study of the in-field dependence of J_c in δ-MoN thin films provides information about the vortex dynamics in superconducting metal nitrides with Gi intermediate between LTS and HTS and IBS.

In this article, we study the vortex dynamics in a 420 nm thick δ-MoN film on (100) Si. The film was grown at room temperature by

* Corresponding author. Comisión Nacional de Energía Atómica and Consejo Nacional de Investigaciones Científicas y Técnicas, Centro Atómico Bariloche, Av. Bustillo 9500, 8400 San Carlos de Bariloche, Argentina.
E-mail address: nhaberk@cab.cnea.gov.ar (N. Haberkorn).

https://doi.org/10.1016/j.ssc.2018.08.017
Received 15 July 2018; Received in revised form 27 August 2018; Accepted 29 August 2018
Available online 07 September 2018

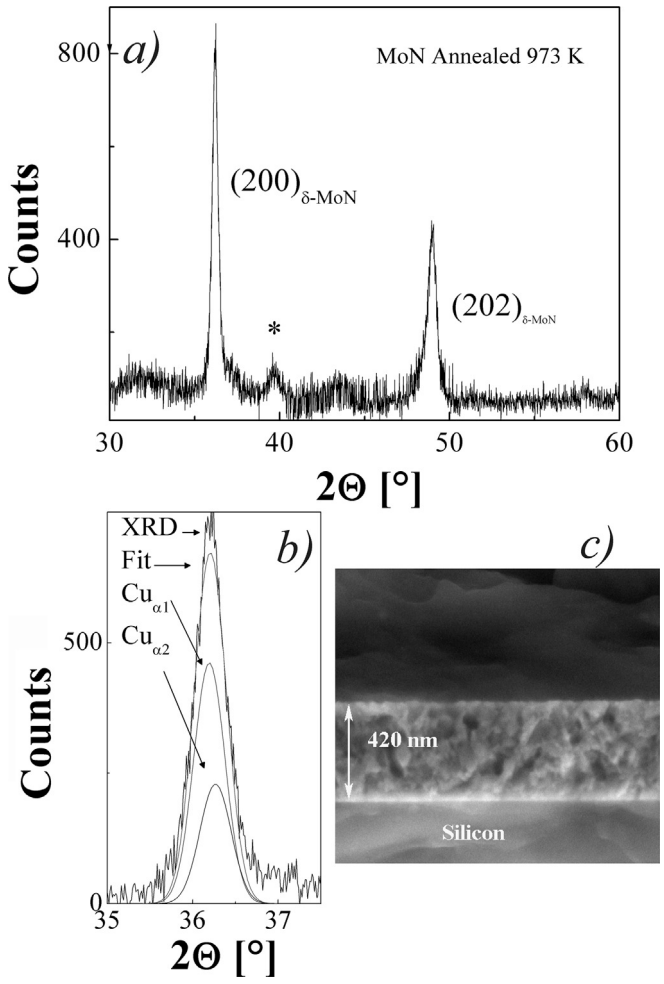

Fig. 1. *a*) X-ray diffraction pattern of a 420 nm thick MoN thin film after annealing at 973 K for one hour. *b*) Deconvolution of the 200 reflection considering Cu $K_{\alpha 1}$ and Cu $K_{\alpha 2}$. (*) corresponds to an unidentified peak. *c*) Cross-section scanning electron microscope image of the film.

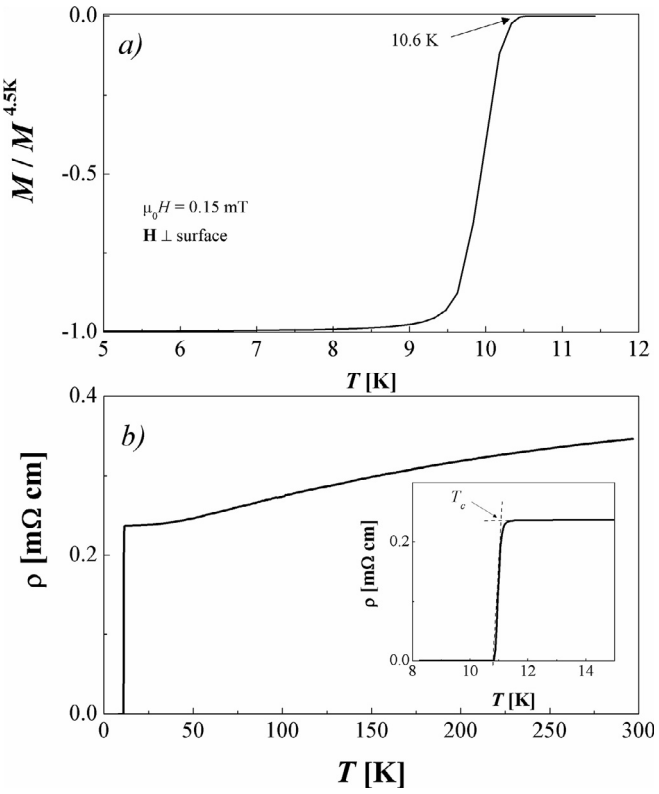

Fig. 2. *a*) Temperature dependence of magnetization with $\mu_0 H = 0.15$ mT. The measurement was performed with **H** perpendicular to the surface. *b*) Temperature dependence of the electrical resistivity. Inset of the figure denotes the methodology to determine T_c.

using reactive sputtering and crystallized at 973 K for one hour in vacuum [11]. After annealing, the film displays δ-MoN phase with grain size $D \approx 30$–65 nm. The self-field J_c at 4.5 K is ≈ 2 MA cm^{-2}. The in-field dependence of J_c at intermediate and low fields (related to the upper critical field) displays a power-law regime. The pinning force F_p displays a maximum at $h = H/H_{irr} \approx 0.3$, which can be related to vortex pinning produced by grain boundaries. Low flux creep rates, described by an Anderson-Kim mechanism, are observed.

2. Material and methods

MoN films were deposited on Si(100) substrates by reactive magnetron sputtering using an $N_2/(Ar + N_2) = 0.5$ mixture without any intentional heating of the substrate [11]. The residual pressure of the chamber was less than 5×10^{-7} Torr. Ultra-high purity Ar (99.999%) and N_2 (99.999%) were used as gas sources. During deposition, the target to substrate distance was ~5.5 cm with 50 W. The total pressure at the chamber was 5 mTorr. The deposition rate was ≈17 nm/min. Thermal annealing was performed in vacuum (to avoid surface contamination) with a residual pressure of 10^{-5} Torr at 973 K during one hour. During thermal annealing, the film was enveloped in a tantalum foil. The results correspond to a 420 nm thick MoN film.

The magnetization (**M**) measurements were performed by using a superconducting quantum interference device (SQUID) magnetometer with the applied magnetic field (**H**) perpendicular to the surface of the film (**H**⊥S). The T_c value (based on magnetization data) was determined from M (T) at $\mu_0 H = 0.15$ mT applied after zero-field cooled (ZFC). The J_c values were calculated from the magnetization data using the appropriate geometrical factor in the Bean Model. For **H** perpendicular to the surface, , where ΔM is the difference in magnetization between the top and bottom branches of the hysteresis loop (length $l >$ width w). The creep rate measurements were recorded for periods of time of one hour. The initial time was adjusted considering the best correlation factor in the log-log fitting of the $\boldsymbol{J_c}$ (t) dependence. The initial critical state for each creep measurement was generated using $\Delta H \sim 4H^*$,

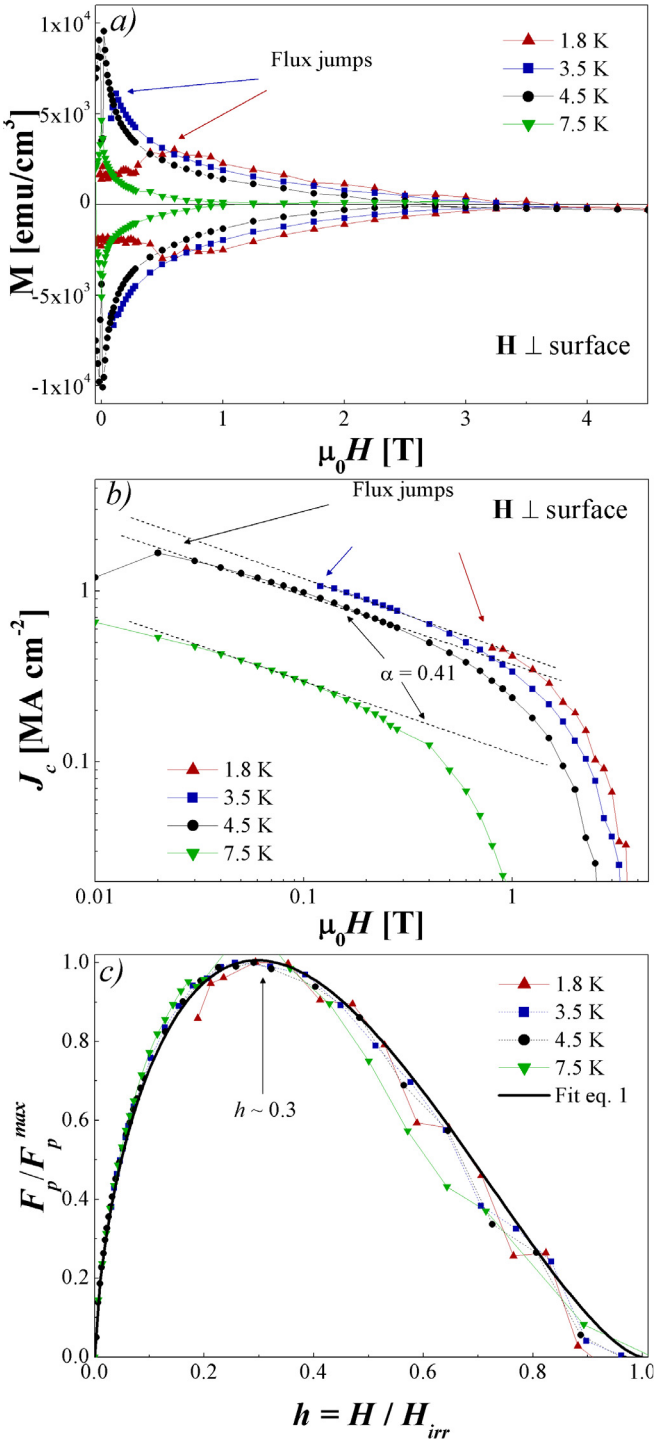

Fig. 3. *a*) Magnetization vs. magnetic field (H) at different temperatures (1.8 K, 3.5 K, 4.5 K, and 7.5 K). *b*) Critical current density (J_c) vs H. *c*) Normalized pinning force (F_p) versus normalized magnetic field [$h = H/H_{irr}(T)$]. All the measurement were performed with **H** applied perpendicular to the surface.

where H^* is the field for full-flux penetration [17].

X-ray diffraction (XRD) patterns were obtained with a Panalitical Empyrean equipment. The electrical transport measurements were performed using the standard four-point configuration.

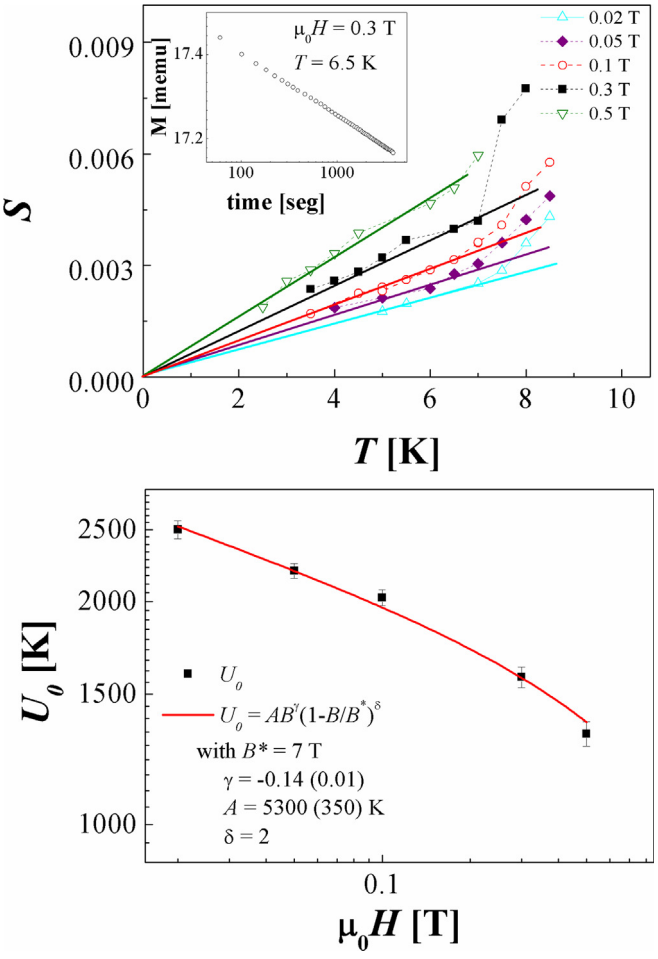

Fig. 4. *a*) Creep rate (S) versus temperature (T) with μ_0H = 0.02 T, 0.05 T, 0.1 T, 0.3 and 0.5 T. Solid lines denote the slope. Inset shows a typical curve of magnetization vs time. All the measurement were performed with **H** applied perpendicular to the surface. *b*) Magnetic field dependence of the flux activation energy U_0.

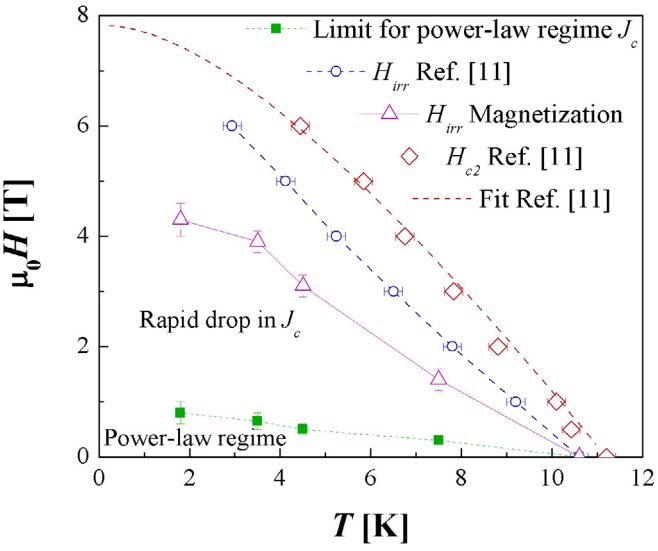

Fig. 5. Magnetic phase diagram for nanocrystalline δ-MoN thin films.

3. Results and discussion

The crystallization of δ-MoN after thermal annealing was confirmed by XRD (see Fig. 1*a*). The lattice parameters calculated from the (200) and (202) diffraction peaks, are $a = 0.571$ (2) nm and $c = 0.562$ (2) nm. The grain size D was estimated from the Scherrer equation (see Fig. 1*b*). The D value depends on the reflection being ≈65 nm and ≈30 nm for the (200) and (202) reflections, respectively. Fig. 1*c* shows a cross-section SEM image. The film thickness is uniform. The image reveals the presence of nanometric grains, which is in agreement with the Scherrer estimation. There are no features that can be related to columnar structures (sources of correlated vortex pinning).

Fig. 2*a* shows the temperature dependence of the magnetization (normalized at 4.5 K) under $\mu_0 H = 0.15$ mT after ZFC. The T_c value obtained at the onset of the magnetization is ≈ 10.6 K. Fig. 2*b* shows the temperature dependence of the resistivity. The MoN film shows a characteristic metallic-like behavior with a residual-resistivity ratio ($RRR = R^{300K}/R^{12\ K}$) = 1.6. As shown in the inset of Fig. Fig. 2*b*, the onset of the superconductivity takes place at T_c of 11.2 K with a transition width of ≈0.5 K. The end of the transition is at 10.7 K, which is in agreement with the magnetization data.

Fig. 3*a* shows magnetic hysteresis loops at 1.8 K, 3.5 K, 4.5 K and 7.5 K. The M (H) at 4.5 K and 7.5 K decreases monotonically with the field. At 1.8 K and 3.5 K, however, the M (H) dependences display irregularities at low fields, as is characteristic of flux jumps. Fig. 3*b* shows the field dependence of J_c obtained from the Bean critical state model. The values for 1.8 K and 3.5 K at low fields (affected by flux jumps) are not included. The $J_c^{H\to 0}$ at 4.5 K is close to 2 MA cm^{-2}. The J_c (H) curves present two clear regimes. At low and intermediate fields the data is described by a power-law regime $J_c\ (H) \propto H^{-\alpha}$ [18]. At high fields, J_c drops quickly, which is usually related to high flux creep rates [19]. The single vortex regime, usually observed as $J_c^{H\to 0} \approx$ constant is not observed [18]. The α value at the different temperatures is ≈ 0.41. The α value depends on the material and of the type of pinning centers. IBS single crystals with random point disorder and normal inclusions show a α ≈ 0.47 [20]. HTS display an α which ranges from 0.55 for nanoparticles to 0.2 for columnar structures [18,19]. The pinning mechanism can be analyzed by the pinning force ($F_P = J_c H$). The $F_p(H, T)$ is scaled as $\frac{F_p}{F_p^{max}} \propto vs\ h$ (with $h = H/H_{irr}(T)$) [21]. Fig. 3*c* shows the F_p/F_p^{max} versus h at different temperatures. The curves are similar with a maximum close to $h \approx 0.3$. This value is in the middle of the expectations for random disorder (0.33) and normal inclusions (0.2) [20]. Considering that the δ-MoN film displays a polycrystalline structure with grain sizes of a few nanometers, it is necessary to contemplate the grain boundaries as a source of pinning [22]. The pinning force considering the relationship between the vortex distance $a_0 = 1.075\left(\frac{\varphi_0}{B}\right)^{1/2}$ and D is given by:

$$F_P = 1.17x10^{11}\left(\frac{H_{c2}^{\frac{5}{2}}}{k^2}\right)h^{\frac{1}{2}}(1-h)^2\frac{\ln\left(1+\frac{D}{a_0}\right)}{\left(1+\frac{D}{a_0}\right)}, \quad [1]$$

where $k = \lambda/\xi$. In this model the position of the maximum in F_p/F_p^{max} versus h depends on the grain size D. The experimental data with $h \approx 0.3$ is well described using a D = 20–30 nm (see Fig. 3*c*). Larger D values in Eq. (1) shift the maximum to lower h [22].

The vortex dynamics was characterized by performing magnetic relaxation measurements. Fig. 4*a* shows the temperature dependence of the flux creep rate $S = -\frac{dlnJ_c}{dlnt}$ for different H. Measurements at $\mu_0 H > 0.5$ T were not performed because the magnetic signal decreases abruptly with the field, and it becomes quite small (most data for $T > 4.5$ K is above the end of the power-law regime). At low temperatures the S values change linearly with the temperature, and this can be described by an Anderson-Kim model with $S = T/U_0$ (with U_0 is the pinning energy barrier) [16]. The $J_c(t)$ dependence varies logarithmically as $J(t) = J(0)\left[1-\left(\frac{T}{U_0}\right)\ln\left(\frac{t}{t_0}\right)\right]$ (with t_0 an effective hopping attempt time). Fig. 5*b* shows the U_0 (H) dependence. The U_0 values range between 2500 K at $\mu_0 H = 0.02$ T and 1300 K at $\mu_0 H = 0.5$ T. A rough estimate of the pinning energy, considering the condensation energy within a coherence volume is given by $U_0 = (H_c/8\pi)^{4}/_{3}\pi\xi^3$ [23] Using the values λ = 300–400 nm for the penetration depth and $\xi = 7$ nm for the coherence length [11] at $T = 0$ gives $U_0 \approx$ 500–1000 K, which is of the same order found in our experimental data. Following Thompson et al. [23], we fit the data using the equation $U_0 = AB^{\gamma}\left(1-\frac{B}{B^*}\right)^{\delta}$ (with B^* the H_{irr}). The exponents γ and δ correspond to the variation due to the reduction of J_c (similar to Fig. 3*c*) and the suppression of the superconducting properties with the field, respectively. The fit, fixing $B^* = 7$ T [11] and δ = 2 (in agreement with the pinning force), gives $A = 5300$ K and $\gamma = -0.14$. A similar parabolic behavior has been previously observed in $NbSe_2$ and MgB_2 [24], and IBS [25]. In our data, the fast decay of U_0 at fields above 0.5 T is directly related to the J_c (H) dependences and the end of the power-law regime (at fields much smaller than H_{irr}).

Fig. 5 shows the H-T phase diagram for nanocrystalline δ-MoN thin films. The H_{c2} and H_{irr} values using electrical transport are included [11]. The H_{irr} (T) obtained by magnetization is significantly smaller than the transport one, which can be related with the low sensitivity of the magnetization to small screening currents. The power-law regime, which is a signature of small flux relaxation rates, is extended to ≈1 T at 1.8 K and decrease significantly to ≈0.5 T at 4.5 K. The vortex lattice constant a_0 for $B = 1$ T corresponds to inter-vortex distances of ≈49 nm, which is similar to the grain size scale.

4. Conclusions

We study the vortex dynamics in nanocrystalline δ-MoN thin films. The microstructure displays grains with sizes between 30 nm and 65 nm. The self-field J_c at 4.5 K is ≈ 2 MA cm^{-2}. The magnetic field dependence of J_c at intermediate and low fields (related to the upper critical field) displays a power-law regime with α = 0.41. The F_p (h) displays a maximum at $h \approx 0.3$, which can be related to vortex pinning produced by grain boundaries. The vortex dynamics is governed by simple Anderson-Kim mechanism. The U_0 values range from ≈2500 K for $\mu_0 H = 0.02$ T to ≈1300 K for $\mu_0 H = 0.5$ T.

Acknowledgments

The authors thank A. Baruj for technical support. This work has been partially supported by Agencia Nacional de Promoción Científica y Tecnológica PICT 2015–2171 and CONICET PIP 2015-0100575CO. N. H. and J. A. H. are members of the Instituto de Nanociencia y Nanotecnología CNEA-CONICET (Argentina).

References

[1] Sergey K. Tolpygo, et al., IEEE Trans. Appl. Supercond. 28 (2018) 1100212.
[2] M. Chandra, Natarajan, et al., Supercond. Sci. Technol. 25 (2012) 063001.
[3] A. Serquis, et al., Supercond. Sci. Technol. 20 (2007) L12–L15.
[4] Y.Y. Zhang, et al., Nanoscale 4 (2012) 2268.
[5] A.B. Karki, et al., Phys. Rev. B 77 (2008) 212503.
[6] Shanmin Wang, et al., Sci. Rep. 5 (2015) 13733.
[7] N. Haberkorn, et al., Supercond. Sci. Technol. 26 (2013) 105023.
[8] D.K. Christen, S.T. Sekula, J.T. Ellis, J.D. Lewis, J.M. Williams, IEEE Trans. Magn. 23 (1987) 1014.
[9] Y.Y. Zhang, et al., J. Am. Chem. Soc. 133 (2011) 20735.
[10] Hanlu Zhang, et al., J. Alloy. Compd. 704 (2017) 453.
[11] N. Haberkorn, et al., Thin Solid Films 660 (2018) 242.
[12] K.E. Gray, R.T. Kampwirth, J.M. Murduck, D.W. Capone, Phys. C 152 (1988) 445.

[13] K. Senapati, N.K. Pandey, Rupali Nagar, R.C. Budhani, Phys. Rev. B 74 (2006) 104514.
[14] A. Pruymboom, W.H.B. Hoondert, H.W. Zandbergen, P.H. Kes, Jpn. J. Appl. Phys. 26 (1987) 1531.
[15] G. Blatter, M.V. Feigel'man, V.B. Geshkenbein, A.I. Larkin, V.M. Vinokur, Rev. Mod. Phys. 66 (1994) 1125.
[16] P.W. Anderson, Y.B. Kim, Rev. Mod. Phys. 36 (1964) 39.
[17] Y. Yeshurun, A.P. Malozemoff, A. Shaulov, Rev. Mod. Phys. 68 (1996) 911.
[18] C.J. van der Beek, et al., Phys. Rev. B 66 (2002) 024523.
[19] N. Haberkorn, et al., Phys. Rev. B 85 (2012) 174504.
[20] N. Haberkorn, Man Jin Eomb, Jung Sang You, Jeehoon Kim, Jun Sung Kim, Solid State Commun. 231–232 (2016) 26.
[21] D. Dew-Hughes, Philos. Mag. A 30 (1974) 293.
[22] Alfred Kahan, Phys. Rev. B 43 (1991) 2678.
[23] J.R. Thompson, et al., Supercond. Sci. Technol. 18 (2005) 970.
[24] S.D. Kaushik, V. Braccini, S. Patnaik, Pramana 71 (2008) 1335.
[25] S. Swati Pandya, Sherif, L.S. Sharath Chandra, V. Ganesan, Supercond. Sci. Technol. 24 (2011) 45011.